

# Rapid differential transport of Nodal and Lefty on sulfated proteoglycan-rich extracellular matrix regulates left-right asymmetry in *Xenopus*

Lindsay Marjoram and Christopher Wright\*

## SUMMARY

The spatiotemporally dynamic distribution of instructive ligands within embryonic tissue, and their feedback antagonists, including inherent stabilities and rates of clearance, are affected by interactions with cell surfaces or extracellular matrix (ECM). Nodal (here, *Xnr1* or Nodal1 in *Xenopus*) and Lefty interact in a cross-regulatory relationship in mesendoderm induction, and are the conserved instructors of left-right (LR) asymmetry in early somitogenesis stage embryos. By expressing *Xnr1* and Lefty proteins that produce mature functional epitope-tagged ligands *in vivo*, we found that ECM is a principal surface of Nodal and Lefty accumulation. We detected Lefty moving faster than Nodal, with evidence that intact sulfated proteoglycans in the ECM facilitate the remarkable long distance movement of Nodal. We propose that Nodal autoregulation substantially aided by rapid ligand transport underlies the anteriorward shift of *Nodal* expression in the left LPM (lateral plate mesoderm), and speculate that the higher levels of chondroitin-sulfate proteoglycan (CSPG) in more mature anterior regions provide directional transport cues. Immunodetection and biochemical analysis showed transfer of Lefty from left LPM to right LPM, providing direct evidence that left-side-derived Lefty is a significant influence in ensuring the continued suppression of right-sided expression of Nodal, maintaining unilateral expression of this conserved determinant of asymmetry.

**KEY WORDS:** Nodal, Lefty, *Xenopus*, Left-right asymmetry, ECM, Sulfated proteoglycans

## INTRODUCTION

Nodal signaling at post-gastrulation stages is the primary conserved regulator of the asymmetric left-right (LR) patterning of the body axis. This process provides the foundation for the large-scale and integrated morphogenetic movements that place the organ anlagen asymmetrically, determine their LR structural differences, and ensure the formation of a stereotypic, unidirectional cardiovascular system (Massagué, 1998; Schier, 2003; Wright, 2001). The pathway defining the left versus right side of the vertebrate embryo involves the expression of *Nodal* (*Xnr1* in *Xenopus*; provisionally renamed *Nodal1*) (Bowes et al., 2010) at the node or an equivalent 'LR coordinator' structure (Ramsdell, 2005), including a transient asymmetric expression in this structure in some species. Signals passed from the node lead to the conserved unilateral left-sided expression of *Nodal/Xnr1* within the left lateral plate mesoderm (LPM), and its downstream target genes: the feedback antagonist gene *Lefty* and the effector transcription factor gene *Pitx2*.

Disruptions in the dynamics of asymmetric *Nodal/Xnr1* expression have been proposed causative in congenital defects of organ placement and structure (Casey, 1998; Casey and Hackett, 2000; Ramsdell, 2005). In current models for LR patterning (Aw and Levin, 2009; Raya and Belmonte, 2006; Tabin, 2006), cross-regulatory positive-negative feedback between Nodal and Lefty causes the asymmetric amplification of initially small LR differences in Nodal signaling intensity, leading to an essentially binary readout with left-sided expression and right-sided absence

of *Nodal* and its effector *Pitx2*. In these models, preventing right-sided *Nodal* expression includes an active suppression effect described below.

The left LPM expression pattern of *Nodal* is dynamic and transient. In *Xenopus*, it shifts rapidly and over a large distance from posterior-to-anterior (P-to-A) and is then shut down, with tissue morphogenesis (e.g. gut bending, cardiac looping) only occurring substantially later. *Xnr1* auto-induction is a major contributor to the forward shifting of the left LPM expression domain, whereas induction of its feedback antagonist Lefty may limit the duration and range of influence of *Nodal* expression (Lowe et al., 1996; Nakamura et al., 2006; Ohi and Wright, 2007; Wang and Yost, 2008; Yamamoto et al., 2003). A self-enhancement and lateral inhibition (SELI) model (Nakamura et al., 2006) has been proposed to explain LR compartmentalization via *Nodal* regulation. SELI invokes a plausible long-range contralateral communication process for establishing and maintaining distinct left (*Nodal-on*) and right (*Nodal-off*) compartments, to enable later embryo-wide integrated morphogenesis. An orthogonal movement of Nodal from the left LPM leads to axial midline expression of *Lefty*. Transfer of Lefty to the right LPM, from both left LPM and axial midline, is proposed as a suppressive, conditioning influence on the contralateral right LPM, blocking the autoregulatory *Nodal* loop (Nakamura et al., 2006; Yamamoto et al., 2003). It has not been determined that Lefty can in fact move to the right side directly from the left LPM, or if the secondary *Lefty* expression zone in the axial midline tissue is more influential. In addition, the degree to which the rapid P-to-A shift of *Xnr1* expression, occurring over about 7 hours, could be explained solely by *Nodal/Xnr1* auto-activation requires investigation of the parameters affecting the ipsilateral range and speed of movement of Nodal and Lefty along the left LPM. The full forward shift of the *Xnr1/Nodal* expression domain is required for anterior structures such as the heart primordium to receive this asymmetric patterning signal.

Department of Cell and Developmental Biology, Program in Developmental Biology, Vanderbilt University Medical School, Nashville, TN 37232, USA.

\* Author for correspondence (chris.wright@vanderbilt.edu)

The cell biological and tissue structural features that facilitate or limit Nodal and Lefty ligand movement at the time of LR asymmetric gene expression should be central determinants of the level and duration of Nodal signaling over the embryo. A future goal is to deduce how broad or more focal regions of tissue experience and act upon the dynamic Nodal signaling activity map. Ligand movement and longevity considerations mean that the extent of Nodal signaling could be badly misjudged based upon RNA expression patterns. Detecting the mature Nodal ligand and characterizing its biochemical behavior would help fill such gaps, hopefully making connections with the tissue patterns of downstream signal transducers (e.g. the canonical nuclear localization of phospho-Smad2) and target genes, and to the locations where asymmetric morphogenesis is initiated.

Studies examining Nodal movement have been hindered by the lack of suitable antibodies, with signal-to-noise ratios being the central problem for ligands operating at low levels in vivo. A general strategy has been to detect overexpressed epitope-tagged variants, or to infer which cells undergo active signaling through phospho-Smad2 or target gene activation patterns (Chen and Schier, 2001; McDowell et al., 1997; Williams et al., 2004). Experiments in blastula-gastrula stage embryos and tissue explants have suggested that Nodal and Lefty can travel several cell diameters from a production source (Branford and Yost, 2002; Cha et al., 2006; Chen and Schier, 2001; Williams et al., 2004), but with sometimes variable findings. *Xnr2* was initially classified as a short-range molecule (Jones et al., 1996) but later as long-range (Williams et al., 2004). The reasons remain obscure, but variations in the tags used or analytical methods possibly lead to different apparent mobilities. With respect to the SELI mechanism, it would be useful to know more about the movement and perdurance of Nodal and Lefty in tailbud stage embryos. The rapidity of tissue maturation during embryogenesis makes it dangerous to assume that such properties are similar in blastula and tailbud stages. In addition, specific aspects of ligand movement in the tailbud/somitogenesis stage embryo, such as through spaces between tissues or along extracellular surfaces, might allow conduit-like, rapid travel to sites far from their source.

Here, we define the LPM tissue architecture in *Xenopus* embryos before and during asymmetric gene expression, finding that it is an unpolarized pseudo-epithelial tissue over the period of maximal *Xnr1* and *Lefty* expression. We describe results with functional epitope-tagged proteins, supplied in limited quantities from grafts, which support the differential speed of *Xnr1* and *Lefty* movement, and a role for ECM in aiding their extremely long-range transport. We discuss the possible significance of these features in constraining *Xnr1* expression to the left LPM, while concurrently promoting the dynamic, rapid P-to-A shifting of the left-sided *Xnr1* expression domain as a determinant of asymmetric morphogenesis.

## MATERIALS AND METHODS

### Embryo manipulation

Albino eggs were fertilized (Cha et al., 2006), embryos staged according to Nieuwkoop and Faber (Nieuwkoop and Faber, 1967), fixed in MEMFA (Sive et al., 2000) from stages 17–45 (2 hours, 23°C or 4°C, overnight) and stored in PBS (cryosectioning) or 100% methanol (in situ analysis).

### Immunofluorescence

Embryos were processed as described by Kucenas et al. (Kucenas et al., 2008), embedded in 3% agar/5% sucrose and transversely cryosectioned (14 µm). Every eighth section (approx. every 100 µm) surveyed the entire anteroposterior axis.

Sections were rehydrated, blocked with 2% NDS (Jackson Immuno)/2% BSA and incubated with the following primary antibodies: ZO1 (Zymed), aPKC\* (Santa Cruz), E-Cadherin (BD Biosciences), β1-Integrin (DSHB), β-Catenin (a generous gift from Pierre McCrea, MD Anderson Cancer Center, TX, USA), Fibronectin (a generous gift from Doug DeSimone, University of Virginia, VA, USA), Laminin (Abcam), HSPG (Seikagaku), CSPG (Sigma), Alexa 488-conjugated Phalloidin (Invitrogen), Myc\* (9E10 mouse monoclonal, Vanderbilt Monoclonal AB Core; Abcam) and Myc\* (rabbit polyclonals: Millipore; Santa Cruz); asterisks signify the use of Neutravidin/Biotin amplification step during IF. Secondary antibodies were: Cy2-, Cy3- or Cy5-conjugated anti-mouse or anti-rabbit secondary antibodies (Jackson Immuno) or DyLight549-conjugated Neutravidin (Pierce). All images were obtained with an Olympus FV-1000 confocal and Fluoview software. To avoid image overprocessing (tagged proteins being supplied in limited amounts), there was no post-processing; panels are best viewed on a monitor, not printed. Signal intensity was analyzed by ImageJ (version 1.43g, NIH) line-scan. Three-pixel line-scans through the LPM or dorsal periaxial regions of each section from embryos with epitope-tagged grafts were compared with background averaged from at least 10 identically processed embryos carrying untagged grafts. Genuine signal threshold was at least 3 s.d. above that average. When signal was lower, the lower background was averaged from 10 three-pixel line-scans within the same section, with 'real signal' again at least 3 s.d. higher.

### Injection constructs

*Lefty*<sup>6MYC-CT</sup> has been reported previously (Westmoreland et al., 2007). *Xnr1*<sup>6MYC-CS</sup> was constructed after 6MYC (containing two glycines and *Ascl* at each end) was PCR-amplified from pCS2+MT (David Turner, University of Michigan, MI, USA) and inserted into an *Ascl* site that was inserted four residues downstream of the cleavage site of *Xnr1* pCS2+. Capped RNA was made by mMessage mMachine (Ambion).

### Animal cap grafts

One-cell albino embryos received 500 pg *Lefty*<sup>UNTAGGED</sup> or *Lefty*<sup>6MYC-CT</sup>, and 250 pg *Xnr1*<sup>UNTAGGED</sup> or *Xnr1*<sup>6MYC-CS</sup> RNA. Stage 9 caps were isolated (Gastromaster, 400 µm square tip), trimmed and engrafted into equivalent pockets (LPM/epidermis removed), midtrunk location, in stage 17 albino embryos (Ohi and Wright, 2007). Embryos were developed for 3–6 hours, fixed (2 hours, MEMFA) and processed for immunofluorescence or in situ hybridization (Ohi and Wright, 2007). mGFP/pCS2+ encodes eGFP with CAAX Ras membrane localization (Wallingford et al., 2000). mGFP-labeled graft removal used Leica fluorescent microscope.

### Xyloside treatment

Dejellied two-cell embryos were treated with 5 mM *p*-nitrophenyl-β-D-xylopyranoside (xyloside; Sigma) in 0.5% DMSO in 0.1× Steinberg's solution until stage 15/16, demembranated, then placed in 10 mM xyloside (1% DMSO, 0.1× Steinberg's). Stage 17 embryos in 0.75× NAM±1 mM xyloside received *Xnr1*<sup>6MYC-CS</sup>/mGFP-expressing AC grafts, and were placed in 10 mM xyloside/1% DMSO for 5 hours, fixed and cryosectioned.

### Western blot

Cell lysates from embryos, LPM explants or AC grafts (Westmoreland et al., 2007) used RIPA buffer with 1% SDS to solubilize more ECM-associated proteins (Dzamba et al., 2009). Primary antibody was rabbit anti-Myc (Millipore); secondary antibody was goat anti-rabbit IgG-HRP (Santa Cruz); chemiluminescent detection was carried out using Super Signal West Femto (Pierce) (see Fig. S6 in the supplementary material).

## RESULTS

### Structure of left and right LPM and ECM composition during tailbud stages

Although LPM has been characterized histologically in several organisms at older stages (Deimling and Drysdale, 2009; Horne-Badovinac et al., 2003; Meier, 1979; Pohl et al., 2005), its layering and epithelial state is poorly understood during the stages of LR gene expression and leading up to asymmetric morphogenesis. To

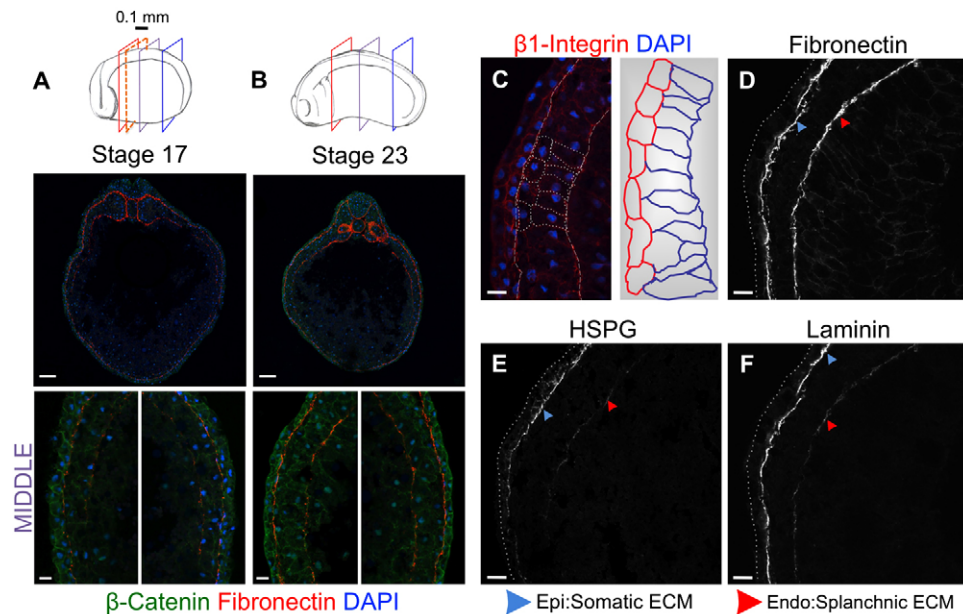


**Fig. 1. Bilayered LPM is LR symmetrical from tailbud-tadpole stages with splanchnic-somatic structural differences beginning at stage 23.** (A, B) Diagrams indicate stage/length and sectional planes. Analysis every 0.1 mm (dashed red frame) was between anterior-posterior LPM extremes indicated by red/blue frames. Representative mid-embryo sections (purple frame) are shown. (A) Stage 17 (10 $\times$ , 40 $\times$ ), left and right LPM each comprising two layers.  $\beta$ -Catenin (green); DAPI (blue). Fibronectin (red) flanks epidermal/endodermal faces of left and right LPM. (B) Stage 23: maintenance of bilayered left and right LPM. (C) Left/right LPMs are structurally similar during these stages, but somatic/splanchnic layers become distinct, symmetrically, from stage 23; somatic cells are more squamous, splanchnic are more columnar. (D-F) Somatic and splanchnic LPM show different basal lamina compositions. Somatic: strong fibronectin, HSPG and Laminin signal; splanchnic: much weaker HSPG/Laminin signal, especially laterally. Scale bars: 100  $\mu$ m, in top images A, B; 20  $\mu$ m in bottom images A, B; 20  $\mu$ m in C-F.

begin to address how tissue architecture or ECM composition affect unilateral *Xnr1* expression, we analyzed LPM before, during and after *Xnr1/Lefty* expression.

We extensively surveyed cell adhesion and ECM proteins within the left and right LPM from early tailbud to early tadpole stages. We used  $\beta$ -catenin, a basolateral marker in polarized epithelia that generically detects cell borders in nonpolarized cells. From stage 17, the cell-surface  $\beta$ -catenin signal showed the LPM beginning to organize into two cell layers with future apical surfaces juxtaposed (Fig. 1A, B; see Fig. S1 in the supplementary material). Similar results were obtained with  $\beta$ 1-integrin, E-cadherin and  $\alpha$ 5-integrin (data not shown), markers that become basolateral when epithelia become polarized. The ECM component fibronectin flanked the somatic and splanchnic left and right LPM (Fig. 1A, B; see Fig. S1 in the supplementary material). Beginning at stage 23, the splanchnic layer in both the left and right LPM began to appear more columnar (Fig. 1C). At the stages examined here, all before the physical separation of splanchnic/somatic layers and coelom opening, these differences were more prominent towards anterior regions, which is probably attributable to the progressive A-to-P maturation of the embryo's mesodermal layer (Slack and Tannahill, 1992). Splanchnic-somatic cell shape differences were maintained through stage 34, the oldest stage examined (see Fig. S1 in the supplementary material).

Because previous studies linked ECM components to the long-range movement of TGF $\beta$  ligands (Belenkaya et al., 2004; Guo and Wang, 2009; Oki et al., 2007; Yu et al., 2009), and establishment of asymmetric organ morphogenesis (Kramer et al., 2002; Kramer and Yost, 2002; Yost, 1990), we assessed the expression of other ECM proteins in the basal lamina of the LPM. Although fibronectin coated the somatic and splanchnic LPM surfaces at

similar levels, other ECM markers were differentially distributed between the epidermal and endodermal interfaces, with apparent LR equivalence (Fig. 1A, B, D-F). Higher levels of laminin and heparan-sulfate proteoglycan (HSPG) were present at the somatic LPM-epidermis interface compared with the splanchnic LPM-endoderm margin (Fig. 1D-F). Up to at least stage 25, chondroitin-sulfate proteoglycan (CSPG) surrounded the notochord and ventral neural tube, and was detected in the ECM of the dorsal endoderm and somite boundaries, with anteriorly enhanced levels and posterior absence (see Fig. S2 in the supplementary material). If the ECM apposing the LPM contained CSPG, it was below the level of sensitivity for this antibody (see Fig. S2 in the supplementary material; not shown). The non-equivalence of the somatic versus splanchnic signal for laminin/HSPG compared with fibronectin was more exaggerated dorsally (Fig. 1E, F). These results suggest that ECM proteins could serve a role in movement facilitation or sequestration of *Xnr1* and *Lefty* ligands, both produced from the LPM.

### Symmetric apical-basal polarization of LPM following asymmetric gene expression

The epithelial character, ECM border characteristics, or apical/basal direction of secretion could influence the route and range of *Xnr1* and *Lefty* transport from the LPM. We therefore examined various markers strongly accepted as diagnostic of apical or basolateral compartments of a polarized epithelium, for a temporal analysis of the polarization state of the LPM.

LPM was characterized with zona occludens 1 (ZO1), a marker of apical tight junctions, between stages 17-34. During the period of asymmetric *Xnr1/Lefty* expression (stages 19-23), apical ZO1 localization was not seen in the left or right LPM anywhere along

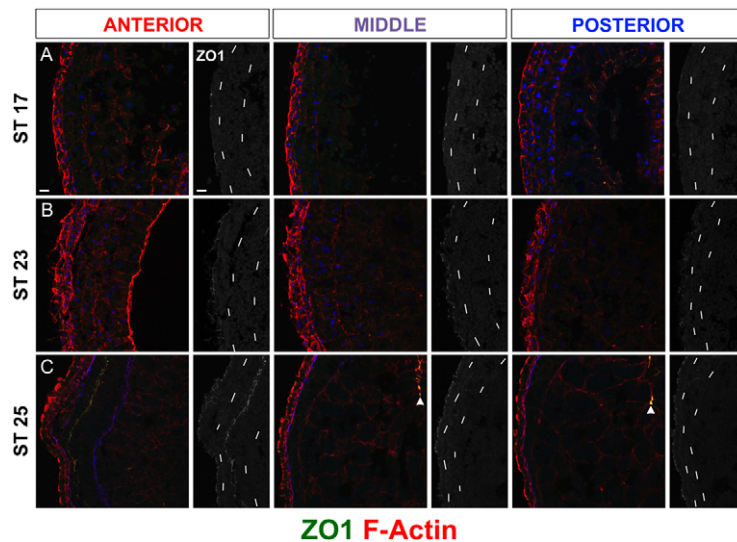


**Fig. 2. LPM undergoes symmetric epithelial polarization after *Xnr1/Lefty* expression.** Anterior, middle and posterior transverse cryosections showing F-actin (Phalloidin, red), ZO1 (green) and nuclei or ECM [blue, DAPI (A,B), Laminin (C)]; 40× images. ZO1 alone (left side shown) is in grayscale, chained lines indicate LPM epidermal/endodermal boundaries. **(A)** Stage 17, LPM is not yet polarized. ZO1 puncta indicate tight junctions in polarized epidermal layer; no puncta are apparent within LPM at stages before asymmetric *Xnr1/Lefty* expression. **(B)** Stage 23, unpolarized LPM during peak *Xnr1/Lefty* expression. **(C)** Stage 25, punctate ZO1 signal appears at somatic/splanchnic interface in anterior left and right LPM; at this stage, asymmetric *Xnr1/Lefty* expression is waning. Arrowheads in C indicate ZO1 in epithelial archenteron. Scale bars: 20 μm.

its length. In the same sections, punctate apical ZO1 was detected in polarized epithelia of the neural tube, epidermis and archenteron (Fig. 2A,B; see Fig. S3 in the supplementary material). Additional apical-specific marker analysis (aPKC, F-actin, Crumbs3; not shown) confirmed the absence of detectable LPM apicobasal polarity between stages 17 and 23.

Beginning at stage 24/25, corresponding to the waning of asymmetric *Xnr1/Lefty* expression, apical ZO1 was seen in the anteriormost 100  $\mu\text{m}$  of the left and right LPM, the region immediately posterior to the pharyngeal arches (Fig. 2C; see Fig. S3 in the supplementary material). Later, the apical ZO1 signal spread progressively posteriorwards in both left and right LPM. At stage 34/35, a point just prior to gut looping, punctate apical ZO1 extended along the entire length of the LPM (see Fig. S3 in the supplementary material). These results suggest that the *Xnr1* and *Lefty* ligands are normally produced predominantly within an apicobasal non-polarized environment, with LPM only becoming polarized after the cessation of asymmetric gene expression.

### Epitope-tagged Xnr1 or Lefty are functional and move rapidly from a graft source

Against this LPM architecture and ECM composition foundation, we sought to determine the parameters of Xnr1 and Lefty transport. Although examination of the endogenous proteins would be most relevant, current antibodies have unfavorable signal-to-noise ratios. We therefore generated several tagged variants of Xnr1 and Lefty (see Fig. S4A,B and Fig. S5A,B in the supplementary material) and tested them for normal function (Sakuma et al., 2002; Westmoreland et al., 2007; Williams et al., 2004). We placed two different tags (6xMyc or eGFP) just C-terminal to the cleavage site (CS) or at a C-terminal (CT) location in Xnr1 and Lefty, and tested them by a grafting method. We showed previously that right-sided placement of Xnr1-expressing LPM grafts initiated a right-sided P-to-A wave of *Xnr1* expression, and that left-sided Lefty grafts blocked the endogenous left-sided *Xnr1* expression wave (Ohi and Wright, 2007). Those previous studies (Ohi and Wright, 2007) used plasmid-loaded LPM grafts in which cells inherit the non-integrated plasmid mosaically, therefore expressing the desired protein unevenly and at low levels (data not shown). With that method, we did not reproducibly immunodetect the tagged protein above the ubiquitous yolk autofluorescence. To overcome this problem, we used RNA-loaded animal cap (AC) grafts as the

source: trimmed AC explants were engrafted into recipient stage 17 embryos in either the left or right LPM, and for cultured for several hours (Fig. 3B). The effects on *Xnr1* gene expression were then analyzed. AC grafts healed into hosts somewhat less seamlessly than LPM grafts, but did not hinder embryonic development. AC grafts injected with *Xnr1* displayed a bulbous morphology, an expected response of AC tissue to a potent mesendoderm inducer, whereas Lefty-injected AC grafts healed into the embryo in a more laminar fashion. Although control grafts carrying membrane-bound GFP (mGFP), did not affect endogenous left-sided *Xnr1* expression (see Fig. S4C in the supplementary material) or gross morphology in stage 45 tadpoles (data not shown), *Xnr1* and Lefty from RNA-injected AC grafts had similar effects to the plasmid-based assays described above. This analysis (see Fig. S4A-C in the supplementary material) led to the selection of tagged variants most similar in function to the untagged versions: *Xnr1*<sup>6MYC-CS</sup> and Lefty<sup>6MYC-CT</sup> (Fig. 3A). Right-sided grafts with *Xnr1*<sup>UNTAGGED</sup> or *Xnr1*<sup>6MYC-CS</sup> initiated a P-to-A wave of *Xnr1* expression, and left-sided AC grafts producing either Lefty<sup>UNTAGGED</sup> or Lefty<sup>6MYC-CT</sup> inhibited equivalently the anteriorward shift of *Xnr1* expression (see Fig. S4C in the supplementary material).

Western blot analysis of host tissue after graft removal showed that the principal form of *Xnr1*<sup>6MYC-CS</sup> and *Lefty*<sup>6MYC-CT</sup> secreted from the graft and transported around the embryo was the mature ligand (important because proprotein cleavage is a determinant of signaling range; Cui et al., 2001), and that both were N-glycosylated (see Fig. S6 in the supplementary material). For *Lefty*, we detected specifically the ‘long isoform’, similar to results from blastula/gastrula embryos, and not a putative short isoform that we proposed (Westmoreland et al., 2007) is an unstable clearance intermediate. Our combined biochemical, immunofluorescence and gene expression data demonstrated that these tagged proteins had an appropriate effect on the host embryo tissue signaling systems in terms of the effect on the expression of *Xnr1* (see Fig. S4C and Fig. S6 in the supplementary material).

We then examined ligand movement from AC grafts producing these functional Xnr1<sup>6MYC-CS</sup> and Lefty<sup>6MYC-CT</sup> proteins. AC-grafted stage 17 embryos were cultured for several hours until stage 24/25, then systematically sectioned and analyzed for Myc signal outside of the graft, the latter identified by membrane-bound mGFP. Both Xnr1<sup>6MYC-CS</sup> and Lefty<sup>6MYC-CT</sup> were readily detected

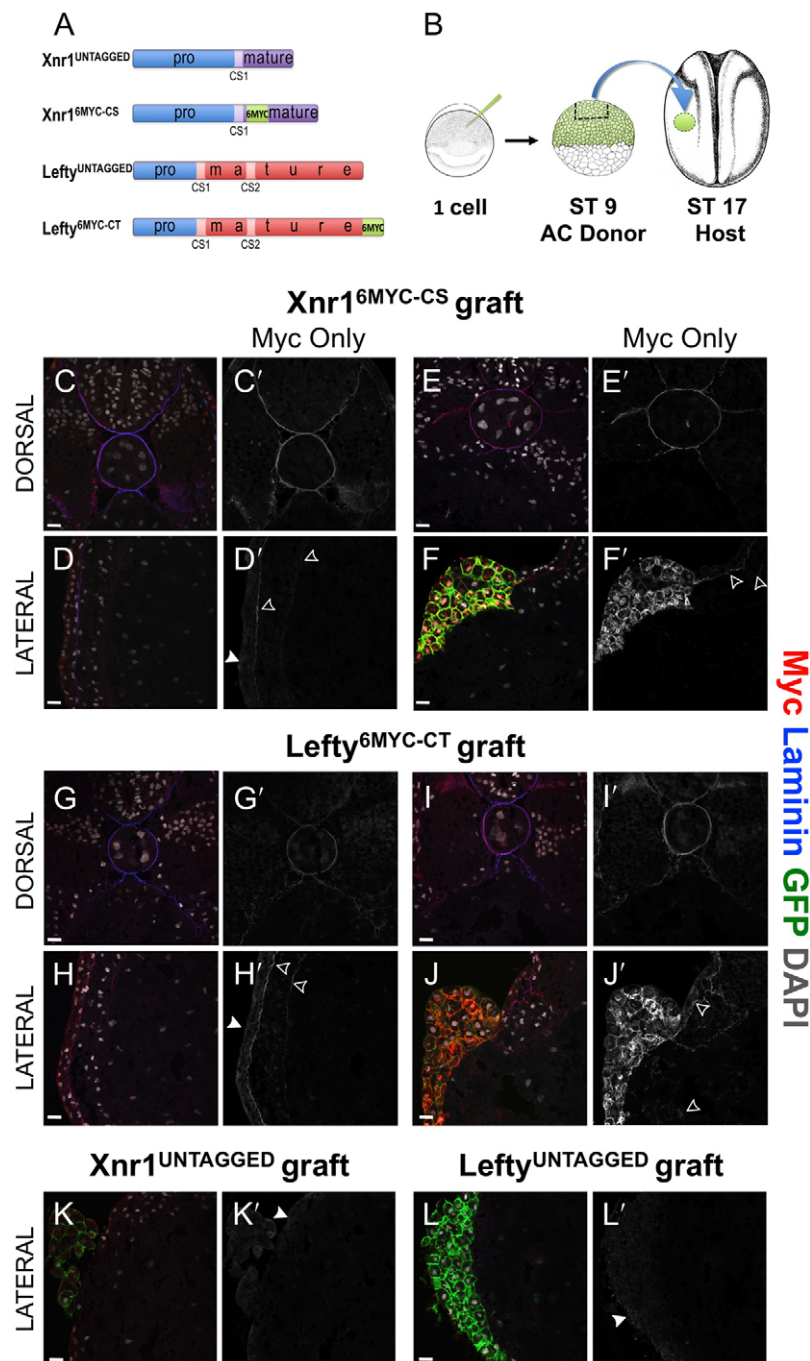


**Fig. 3. Xnr1<sup>6MYC-CS</sup> and Lefty<sup>6MYC-CT</sup> move substantially from AC grafts.** (A) Xnr1 and Lefty constructs: blue box, pro-domain; CS1/CS2, cleavage sites liberating mature ligands; 6MYC tag was inserted just downstream of CS1 (Xnr1) or C-terminally (Lefty). (B) AC-grafting schematic. (C-L') Transverse cryosections were used to detect Myc (red; grayscale in C'-L'), laminin (blue) and nuclei (DAPI, white); dorsal panels focus axially/paraxially, lateral panels on LPM. Membrane-bound GFP (mGFP, green) marks engrafted cells; 2.5  $\mu$ m optical sections. Open arrowheads, Myc; closed arrowheads, nonspecific epidermal haze. (C-F') Xnr1<sup>6MYC-CS</sup>, (G-J') Lefty<sup>6MYC-CT</sup>, (K,K') Xnr1<sup>UNTAGGED</sup> and (L,L') Lefty<sup>UNTAGGED</sup>. (C,C',D,D') Representative section ~110  $\mu$ m anterior of graft margin; Xnr1<sup>6MYC-CS</sup> signal in basal lamina surrounding notochord/neural tube. Dorsal and left LPM Xnr1<sup>6MYC-CS</sup> signal colocalized with laminin. (E,E',F,F') Representative images, dorsal and lateral Xnr1<sup>6MYC-CS</sup> signal within/near graft. Note absence of endoderm signal. (G,G',H,H') Lefty<sup>6MYC-CT</sup> signal colocalized with laminin in dorsal and lateral views, ~340  $\mu$ m anterior of graft. (I,I',J,J') Dorsal and lateral images of Lefty<sup>6MYC-CT</sup> signal. Note Lefty<sup>6MYC-CT</sup> signal is within endoderm, not colocalized with laminin. (K-L') AC grafts with Xnr1<sup>UNTAGGED</sup> or Lefty<sup>UNTAGGED</sup> reveal artefactual hazy epidermal signal (closed arrowheads). Scale bars: 25  $\mu$ m.

both within and outside the graft source. Outside, there was colocalization with the ECM proteins laminin, HSPG and fibronectin (Fig. 3; data not shown). It is important to note that ligand localization was more robustly detected on ECM found at the somatic LPM:epidermal interface relative to signal detected at the splanchnic:endodermal interface or interstitial signal between LPM cells. Xnr1<sup>6MYC-CS</sup> and Lefty<sup>6MYC-CT</sup> were detected at ECM interfaces flanking the left LPM, and around the dorsal periaxial, paraxial and neural structures (notochord, somites and ventral neural tube, respectively; Fig. 3C-J'). We also detected interstitial signal within the LPM, albeit lower than at the ECM interfaces. Identical processing for Xnr1<sup>UNTAGGED</sup> and Lefty<sup>UNTAGGED</sup> AC-grafted embryos (details in the Materials and methods) established

the background against which to evaluate real Myc signal (Fig. 3K-L'; see Fig. S5A-D in the supplementary material). The only substantive background problem was a non-specific epidermal haze (Fig. 3K-L'), becoming more apparent if images were post-processed to enhance Myc signal intensity (see Fig. S5C,D in the supplementary material), which precluded us deciding that ligand moved into the epidermal layer rather than remaining excluded. In sections that contained the graft, or nearby, Lefty<sup>6MYC-CT</sup> was detected interstitially in the adjacent endodermal mass, with an apparently intracellular signal in some cells (Fig. 3J'). Moreover, a Lefty<sup>6MYC-CT</sup> signal was definitely detected at the ECM interface flanking the right LPM, suggesting the long-range, direct contralateral transfer of Lefty from the left-sided graft. This right-

sided transfer was confirmed biochemically (see Fig. S7C in the supplementary material). Although AC engraftment inevitably leads to a reduction (possibly transient) in ECM quality at the LPM-endoderm interface, notably, unlike Lefty<sup>6MYC-CT</sup>, Xnr1<sup>6MYC-CS</sup> was undetectable by immunofluorescence or biochemical analysis in the endoderm or right LPM (see Fig. S7B in the supplementary material). The timing and fractional contralateral transfer of Lefty<sup>6MYC-CT</sup> to the right LPM was addressed. Mature Lefty ligand was present predominantly in the left LPM at 3 hours with a high transfer to the right LPM by 6 hours (see Fig. S7D in the supplementary material). Thus, Lefty has a much greater capacity than Xnr1 to move from LPM AC grafts into the endoderm and towards the right LPM. As discussed more below, the affinity of Nodal and Lefty for the ECM adjacent to the LPM cells secreting these ligands may facilitate their rapid, far-ranging, planar movement. At the same time, the retention of Xnr1 in proximity to the LPM, the responsive tissue, would enable appropriate threshold-dependent regulation of gene expression.

### Epitope-tagged Xnr1 and Lefty clearance

One caveat in studying misexpressed tagged ligands is what the signal represents: 'active protein', or accumulated overly stabilized inactive protein undergoing clearance or terminal sequestration. Although previous experiments by Sakuma et al. (Sakuma et al., 2002) generated useful information on the long-distance transport of Lefty relative to Nodal, these experiments did not include a biochemical analysis of proper ligand cleavage or clearance. To buttress the significance of the Xnr1 and Lefty signals as related to active transport and signaling, we devised an approach to show that the signal does not represent accumulated protein, and that both Xnr1 and Lefty are being cleared relatively dynamically. The visualization of mGFP-expressing AC grafts aided their removal from host embryos after 'ligand-conditioning' the LPM. Embryos received AC Xnr1<sup>6MYC-CS</sup> or Lefty<sup>6MYC-CT</sup> grafts plus mGFP, and were cultured (4.5 hours for Xnr1<sup>6MYC-CS</sup>, 3 hours for Lefty<sup>6MYC-CT</sup>) before the graft was removed. Embryos were fixed immediately (reference peak signal), or 30 or 90 minutes after graft removal, and analyzed for periaxial Myc signal (Fig. 4). Both Xnr1<sup>6MYC-CS</sup> and Lefty<sup>6MYC-CT</sup> signals were principally at periaxial and left LPM ECM. At T30, the Xnr1<sup>6MYC-CS</sup> signal was decreased 60%, and Lefty<sup>6MYC-CT</sup> by 40%, suggesting that, in the absence of continued replenishment from the AC graft, both ligands were effectively cleared. By T90, ~90% of Xnr1<sup>6MYC-CS</sup> and 80% of Lefty<sup>6MYC-CT</sup> signal had disappeared. From this analysis, relative half-lives were inferred as ~25 minutes for Xnr1<sup>6MYC-CS</sup> and 45 minutes for Lefty<sup>6MYC-CT</sup>.

### Lefty travels more rapidly than Xnr1

A key postulate in the reaction-diffusion model for interactions between an inducer (Nodal/Xnr1) and its feedback antagonist (Lefty) in limiting the range/longevity of the inducer's influence is that the antagonist travels faster than its inducer (Turing, 1990). We therefore addressed the rate and distance of movement in intact embryos during the stages of asymmetric gene expression, especially with reference to the types of tissue transport routes that are used. We performed a time-course comparison of the ability of tagged Xnr1 and Lefty to exit grafts and take a dorsal (producing a periaxial signal around notochord and ventral neural tube) or lateral route (planar movement along left LPM surfaces), both anteriorly and posteriorly; measurement of anterior and posterior dorsal ligand transport does not include the distance traveled from the graft to periaxial ECM.

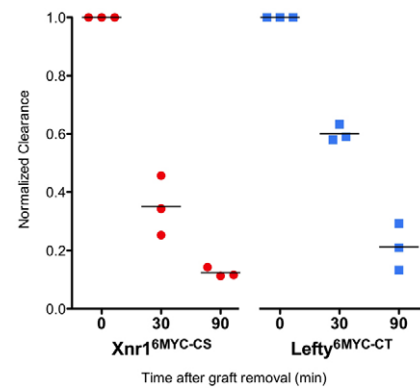


**Fig. 4. Xnr1 and Lefty clearance.** Xnr1<sup>6MYC-CS</sup> (red) and Lefty<sup>6MYC-CT</sup> (blue) clearance was measured by conditioning embryos by engrafting for 3 hours, graft removal and analysis (ImageJ line-scan) 0, 30, or 90 minutes post-removal, values normalized to T0.

At 3 hours post-engraftment (hours PE), dramatic differences were observed between Xnr1 and Lefty. For both ligands, Myc signal was detected in a graded fashion away from the graft, potentially displaying first-order diffusion characteristics, although a careful quantitative biochemical analysis would be required to address this issue (immunofluorescence assays on localized signals are at best semi-quantitative). For the lateral LPM ECM route, anteriorward Lefty<sup>6MYC-CT</sup> movement was twice that of Xnr1<sup>6MYC-CS</sup>, and posterior Lefty<sup>6MYC-CT</sup> signal was detected five times farther than for Xnr1<sup>6MYC-CS</sup> (Fig. 5). This difference was observed for the anteriorward dorsal-periaxial route at 3 hours PE, Lefty<sup>6MYC-CT</sup> having traveled about three times farther than Xnr1. A similar trend was observed for the posterior periaxial route. From these results, we infer an inherent difference in these functional tagged ligands: Lefty travels significantly greater distances in a shorter time period compared with Xnr1. By 5 hours PE, the distances reached anteriorly and posteriorly in the LPM and periaxial regions by Xnr1<sup>6MYC-CS</sup> and Lefty<sup>6MYC-CT</sup> were relatively similar (Fig. 5), implying movement up to 700  $\mu$ m from the source (Fig. 5). The long-range transport and 'catch-up' by Xnr1 compared with Lefty were under conditions of prolonged ligand production from the graft and did not result from ligand accumulation, as shown by the clearance findings above. The later 'catch up' of Xnr1 to Lefty may be related to the ligands reaching some type of anterior and posterior tissue limit; we did not detect signal extending posteriorly into the region of nascent mesoderm formation or anterior of the LPM in the pharyngeal arches or presumptive cardiac field.

### Xnr1 requires sulfated proteoglycans for fast planar LPM transport and dorsalward movement to the midline

Previously, sulfated glycosaminoglycans (sGAGs) were implicated in transporting Nodal from the node to the left LPM in mouse, and sGAG-depleted mouse embryos fail to express left LPM *Nodal*, despite the normal perinodal *Nodal* expression (Oki et al., 2007). Here, we have examined how sGAG removal might affect Xnr1 movement within and from the LPM. Xyloside (*p*-nitrophenyl- $\beta$ -D-xylopyranoside) blocks sGAG attachment by competing with xylosylated core proteins as substrate for galactosyltransferase I, with differential effects on heparan- and chondroitin-sulfate pathways. Preferential binding to CS groups blocks CSPG synthesis, and a lower affinity for HS reduces HSPG synthesis

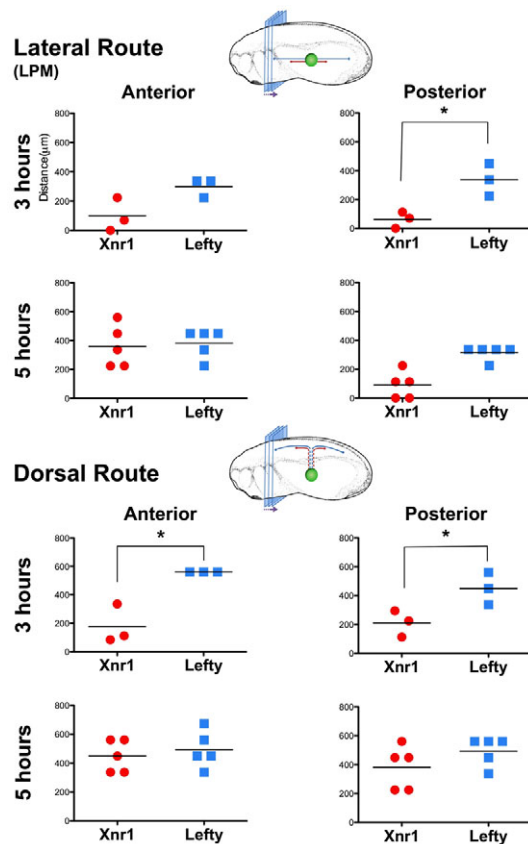


**Fig. 5. *Lefty*<sup>6MYC-CT</sup> travels farther and more rapidly than *Xnr1*<sup>6MYC-CS</sup>.** Diagrammatic representations depict the serial sectional analysis applied and routes measured. Distance of signal detection from graft (ImageJ line-scan) of consecutive dorsal and lateral views, analyzed at 40× magnification. Dorsal transport route measurements do not include the distance from AC graft to periaxial ECM (see Results for detail). Note different distances traveled periaxially and laterally between *Xnr1* and *Lefty* at 3 hours. \*Non-parametric Mann-Whitney test;  $P \leq 0.05$ .

more moderately (Lugemwa and Esko, 1991; Oki et al., 2007). For our analysis here, it is relevant that heparan-sulfate-xyloside conjugates are still secreted and may be detected by immunofluorescence (Stevens and Austen, 1982). Although xyloside prevents proper cardiac looping in frog embryos (Yost, 1990), it has not been determined how sGAG removal alters ligand movement or, specifically in frogs, its effect on the spatiotemporally dynamic expression of *Xnr1*.

We first tested whether xyloside prevented the left-sided LPM initiation of *Xnr1* expression, presumably by blocking transfer of signals from the posterior LR coordinator (gastrocoel roof plate, the equivalent of the late node in the mouse) (Schweickert et al., 2007), a block expected if asymmetric signal transfer to left LPM requires sGAG as in the mouse (Oki et al., 2007). This effect was indeed detected (Fig. 6A,B). The efficiency of sGAG removal was confirmed by analyzing CSPG and HSPG in tissue sections. Embryos treated with xyloside continuously from the two-cell stage completely lacked the CSPG signal in ECM (Fig. 6C,D), and therefore completely removed the ‘anterior enhancement’ of CSPG seen around dorsal periaxial structures (Fig. 6C,D; see Fig. S2 in the supplementary material). HSPG was still detected, but we note with respect to the caveat above that the current antibody and immunodetection methods might not detect fractional reductions in

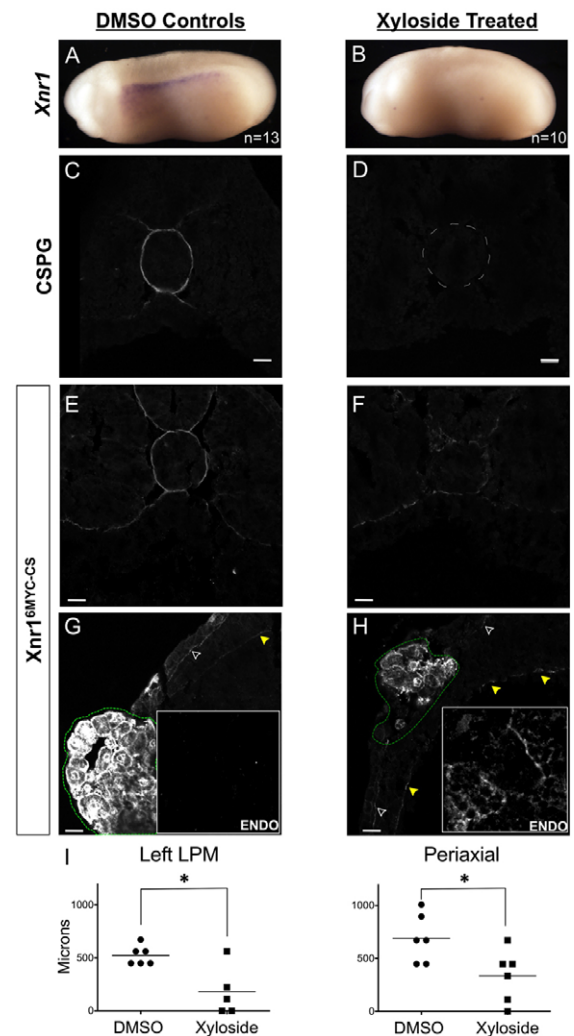


**Fig. 6. Xyloside decreases left LPM-restraint of *Xnr1* signal and alters the distance traveled.** (A,B) Endogenous *Xnr1* expression in left LPM of controls but complete absence from 80% of xyloside-treated embryos. (C,D) CSPG is found periaxially (around notochord) and at the somite/dorsal endoderm interface in DMSO-treated ( $n=9$ ) embryos but is absent from all xyloside-treated embryos ( $n=11$ ). (E,F) *Xnr1*<sup>6MYC-CS</sup> grafts display dorsal periaxial signal, which is markedly reduced with xyloside treatment. (G,H) Dorsolateral left LPM signal on ECM in controls and lack of endodermal signal (inset; graft, green outline). Xyloside-treated *Xnr1*<sup>6MYC-CS</sup> engrafted embryos showed increased endoderm signal (inset), interstitial and intracellular. Note increased relative signal at splanchnic: endodermal ECM. Open arrowheads, epidermal: somatic ECM; yellow arrowheads, splanchnic: endodermal ECM. (I) Xyloside treatment reduces distance traveled by *Xnr1*<sup>6MYC-CS</sup> along lateral and periaxial routes (Fig. 4). \*Non-parametric Mann-Whitney test;  $P \leq 0.05$ . Scale bars: 25  $\mu$ m.

HSPG. The relevance to HSPG is reduced because previous studies have shown that Nodal interacts with CSPG and not HSPG (Oki et al., 2007).

The absence of endogenous asymmetric gene expression in the presence of xyloside provided an opportunity to test how sGAG deficits affected ligand movement from an AC graft in the absence of endogenous ligands produced within the LPM. Because *Xnr1* is the inducer, and *Lefty* the responsive gene, we focused analysis on the movement of *Xnr1*<sup>6MYC-CS</sup>. Control and xyloside-treated

recipients received, at stage 17, AC grafts producing Xnr1<sup>6MYC-CS</sup> and mGFP, and were cultured for 5 hours in the presence/absence of xyloside, a period appropriate to detect an altered speed and range of movement, based upon results described above. Grafted xyloside-treated embryos showed a mislocalization of Xnr1<sup>6MYC-CS</sup>. In many cases, Xnr1<sup>6MYC-CS</sup> was detected interstitially within the endodermal mass, unlike controls (compare Fig. 3D',F' with Fig. 6E-H). Although non-xyloside-treated controls displayed long-distance Xnr1<sup>6MYC-CS</sup> movement along ECM in the left LPM and to periaxial tissues after 5 hours (Fig. 6I), the ratio of signal seen at LPM interfaces was reversed within sGAG-deficient embryos with more signal localized to the splanchnic-endodermal ECM, which may explain the appearance of signal within the endoderm. With respect to ligand movement, xyloside-treated embryos displayed significantly decreased transfer along both dorsal-periaxial and lateral routes (Fig. 6F,H,I). We note that colocalization of tagged Xnr1 with ECM was not abolished, as many other ECM proteins are still present after sGAG depletion, suggesting that low-affinity interactions between Xnr1<sup>6MYC-CS</sup> and yet-undetermined ECM proteins persisted. Analysis of conditioned medium collected from Xnr1<sup>6MYC-CS</sup>-injected ACs cultured in the presence or absence of xyloside showed equivalent secretion of tagged Xnr1. Therefore, xyloside treatment did not alter the production or secretion of tagged Xnr1 from an AC graft. Moreover, despite the mislocalized signal with xyloside treatments, the signal remaining ECM-associated plus that in endoderm (under identical imaging) also suggests that secretion per se was not grossly affected. As well as suggesting that ligand moves faster and farther on sGAG-rich ECM, we hypothesize an additional role in preventing too much Xnr1 from leaving the vicinity of the left LPM, with the premise that threshold signaling is central to enabling an efficient autoregulation-based spatial propagation of *Xnr1* expression.

## DISCUSSION

Few studies exist of Nodal and Lefty movement during the stages of embryogenesis relevant to their asymmetric expression period (Hamada, 2008). It is likely, especially given our results, that ligand movement in blastula-gastrula stages is different from that in tailbud-somitogenesis embryos. Studies on focally secreted GFP-tagged mouse Nodal and Lefty2 in chicken embryos implied that both move far, with Lefty2 traveling farther and faster, supporting a reaction-diffusion relationship (Sakuma et al., 2002; Turing, 1990). More recently, however, movement of tagged Nodal from the node was difficult to detect (Oki et al., 2007). Our findings extend our knowledge of LR signaling processes driven by Nodal/Lefty, by increasing our understanding of the features affecting tissue penetration and activity of this critical ligand pair. We generated biochemical evidence for the proper cleavage and glycosylation of tagged ligands secreted from AC grafts, measured faster relative movement of Lefty compared with Xnr1, and detected a transfer along CSPG/HSPG-rich ECM that we propose is central to the fast directional expansion and shut-down of *Xnr1* expression within left LPM (Fig. 7). Our findings provide a foundation for a future biochemical dissection of ECM-ligand interactions, including determining the relevant structural features, and if there are, for example, differential on-off rates and affinities for CSPG compared with other proteoglycans.

## ECM and Nodal signaling

ECM interactions of several TGF $\beta$ -family ligands affect tissue transport or cell accessibility either positively (facilitation) or negatively (sequestration) (Bernfield et al., 1999). A permissive

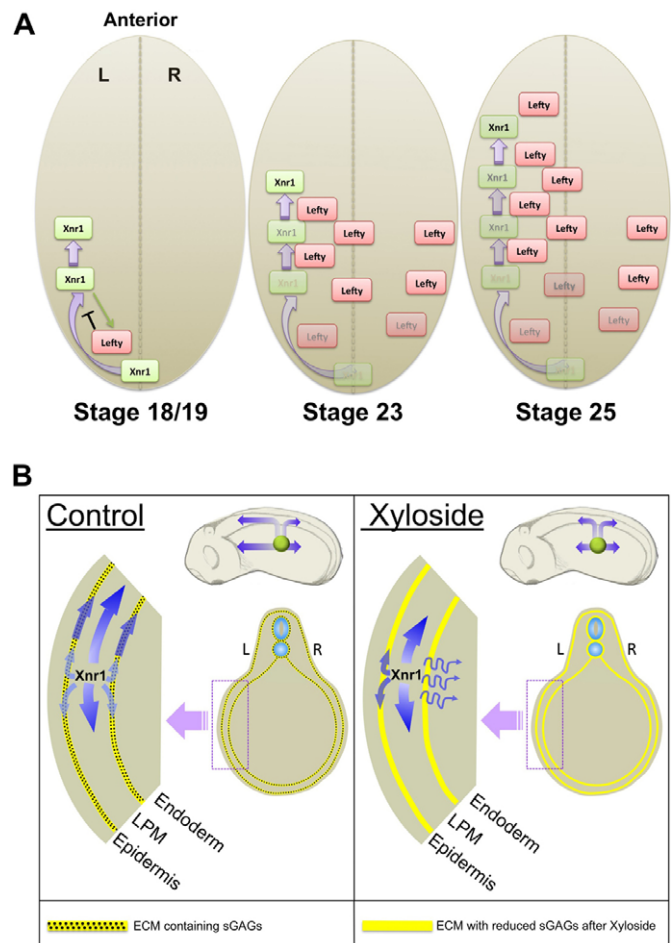


**Fig. 7. Model for effect of sulfated glycosaminoglycans (sGAGs) during asymmetric gene expression.** (A) Asymmetrically-produced Xnr1 in the left LPM beginning at stage 18/19 begins to move

anteriorwards, concentrated over ECM of left LPM/periaxial tissue surfaces, and begins to induce Lefty. Lefty travels anteriorly along left LPM/periaxial ECM more rapidly than does Xnr1, and into endoderm. Lefty catches up to Xnr1, shutting down Xnr1 autoregulation. Lefty stability may prevent a second Xnr1 wave from initiating. (B) sGAGs (stippling) within LPM and periaxial ECM (yellow line) help retain a significant fraction of Xnr1 in proximity to left LPM, while Lefty (not shown) moves more freely to right LPM either directly through endoderm or 'up-and-over' the dorsal axial midline. sGAG removal allows lateral travel of Xnr1 into endoderm, reducing LPM signal and planar movement. This orthogonal transfer reduces the strength of Xnr1 autoregulation within the LPM.

role for heparan sulfate in mesoderm induction mediated by activin was reported (Itoh and Sokol, 1994). In *Drosophila* and mouse, sulfated proteoglycans aid in transporting BMPs, FGFs and Nodal (Belenkaya et al., 2004; Bernfield et al., 1999; García-García and Anderson, 2003; Ohkawara et al., 2002; Oki et al., 2007; Scholpp and Brand, 2004; Yu et al., 2009). A conserved HSPG-binding motif identified as an N-terminal basic residue region in some BMPs (Ohkawara et al., 2002) is absent from Xnr ligands, and it is possible that multiple, distributed low-affinity interactions mediate ECM-binding in other TGF $\beta$  ligands. Ligand range was explored in the zebrafish Nodal ligands, Cyclops and Squint. Acidic residues in the N-terminal region of Squint but absent from Cyclops, proposed to confer long-range capacity (Jing et al., 2006), are not

conserved in Xnrs. We speculate that mature-region Nodal glycosylation, present only in some vertebrates (Le Good et al., 2005), could significantly affect ECM binding (on-off rate, affinity), which (as discussed below) may be particularly relevant in *Xenopus*. The evidence from pharmacological inhibition of sGAG modification that CSPG and potentially HSPG aid the rapid movement of Xnr1 over extensive distances, possibly with a superimposed directional bias, highlights the importance of extracellular spatial regulation of ligand function.

Apicobasal polarization of LPM and separation into distinct somatic and splanchnic layers occurs only after *Xnr1/Lefty* asymmetric expression, meaning that we currently rule out a role for polarized secretion of ligands through specific cell surfaces. Indeed, although ECM showed the highest epitope-tagged Xnr1 signal, it was also distributed around most, possibly all, LPM cells. We currently speculate on a dual role for LPM-flanking ECM: first, to help Xnr1/Nodal move rapidly in the plane of the LPM, both anteriorly and orthogonally towards the dorsal midline (discussed more below); and second, to keep the level of Nodal in the vicinity of the responsive LPM high enough to maintain its feedforward loop, which underlies the expansion of *Xnr1* expression (Ohi and Wright, 2007). These features are important for the relatively unstable Nodal, and less so for the more stable Lefty, which has the ability to depart the ECM and move contralaterally to prevent spurious activation of *Nodal* expression in the right LPM. The high fractional transfer (see Fig. S7D in the supplementary material) suggests that Lefty produced in spatially restricted fashion could have the remarkable ability to bathe large areas of the embryo, for a significant period, in an anti-Nodal suppressive influence.

We hypothesize that dorsalward movement of Xnr1 from the LPM to the midline, which is necessary for inducing axial tissue expression of *Lefty*, is aided by the relative progressive dorsal enrichment of CSPG/HSPG-containing ECM in LPM, and around axial/periaxial tissues. Although not detected with the current antibody, the dorsal CSPG (see Fig. S2 in the supplementary material) could extend lateroventrally, in a graded fashion, towards the splanchnic LPM/endoderm interface, therefore representing a significant directional attractive influence on Xnr1 and Lefty. Ligand flux up this 'ECM gradient' may bring Nodal rapidly to the axial midline where it induces a secondary source of Lefty that can also move towards right LPM.

We also suggest that transport facilitation by dorsally biased CSPG/HSPG within the LPM is overlain by an anteriorward CSPG enrichment, especially noticeable periaxially and correlated to the greater maturity of more rostral regions. Biased ligand movement along both ECM gradients, working together with the relatively high ventral levels of BMP (Hemmati-Brivanlou and Thomsen, 1995), which suppresses Nodal autoregulation, could be major influences defining the dynamic *Xnr1* expression domain. Future real-time tracking of molecular movement, or pulse-chase labeling, might allow more direct determination of routes and range of movement. We might also assess the relative amount of Xnr1 that moves anteriorly only along LPM, compared with moving orthogonally towards axial regions then forward along the CSPG/HSPG tissue-maturity gradient, to return to the dorsal LPM slightly more anteriorly. The latter route could intensify *Xnr1* expression in dorsal LPM, a feature of endogenous *Xnr1* expression (Ohi and Wright, 2007; Sampath et al., 1997), as well as help generate an anteriorward sweep to the Xnr1 auto-activation loop.

## Lefty travels farther than Xnr1, with different tissue penetration

Our data further support a reaction-diffusion relationship between Xnr1/Nodal and Lefty during LR patterning, because the feedback antagonist Lefty moves faster and is more stable, than the Xnr1 inducer (Nakamura et al., 2006; Sakuma et al., 2002; Turing, 1990). These properties in Lefty are probably important in limiting the time and range of influence of Nodal by suppressing its autoregulation and finally terminating its expression. In the SELI model (Nakamura et al., 2006; Tabin, 2006), left-sided *Nodal* self-amplification drives expansion of unilateral expression, and right-sided contralateral *Lefty*-mediated suppression is critical for its 'left-on, right-off' pattern. In *Xenopus* embryos, after an asymmetric signal is received from the posterior LR coordinator region, *Xnr1* expression initiates in posterior left LPM, and begins expanding anteriorly ahead of the expression of *Lefty*. Too brief a delay between *Nodal* and *Lefty* expression, or inappropriate relative movement of inducer and antagonist, would be deleterious. The lack of a timing advantage to *Xnr1* expression would allow Lefty to set off too fast, rapidly squelch Xnr1 feedforward auto-activation, and prevent asymmetric signaling from reaching far enough forward to pattern the cardiac anlage, or even less anterior tissues. Or, Lefty might move to the axial midline too quickly, prevent the orthogonal Nodal-induced *Lefty* expression, and reducing or removing its contribution to the contralateral suppression of *Xnr1* expression, confuse LR patterning almost immediately. Within this framework, the significant transfer of Lefty to the right LPM after production from left-sided grafts provides direct evidence for an embryo-wide transfer of Lefty. We note, however, that the relative amount of Lefty moving directly through the endoderm or 'up-and-over' the dorsal axial midline were not determined, and both paths could contribute meaningfully.

We detected a 'loosening effect' on Xnr1 ligand accumulation on ECM when sGAG modification was xyloside-blocked. Ligand signal was reduced on the ECM facing the epidermis and in dorsal periaxial regions, concomitantly increased on splanchnic-endodermal ECM, and detected permeating the interstitial space within endoderm. This loosening effect greatly reduced the overall range and speed of Xnr1 movement. We suggest that such ECM interactions are a substantial directional transport influence, and plausibly explain how a rapid anterior shift of *Xnr1* expression along LPM could be driven solely by auto-activation. We note that in the different context of blastula/gastrula-stage AC tissue, a loosening effect of ECM disruption was proposed to explain the increased range of Xnr2 (inferred by target gene response) in 'dissociated then reaggregated' explants compared with non-dissociated ones (Jones et al., 1996).

Ultimately, a complete understanding of LR patterning will include linking the threshold-dependent shaping of a spatiotemporally dynamic 'Nodal activity contour map' to the cell biological initiation of asymmetric morphogenesis. In different species, the activity map could be related to specific tissue structure and ECM distribution/composition, which may have become adapted to each other in accordance with the embryo's morphology, size and developmental strategy. Similar influences to those detected here might exist in non-vertebrates that use Nodal signaling to regulate asymmetric embryogenesis.

One should not underestimate the relevance of an ECM-facilitated transfer of ligands within embryos the size of *Xenopus*, which increase in length from 1.5 to 2.8 mm during the ~7 hour period of *Xnr1* expression (stages 19-25), with LPM lengthening from ~0.8 to 1.3 mm. We have previously suggested that Nodal

autoregulation, working only by cell-to-cell-to-cell relay, might be incapable of working fast enough to expand the *Xnr1* expression domain along the entire LPM within this short time. Despite the significant embryo extension, our clearance estimates (Fig. 4) imply that passive ligand conveyance on cells moving away from the AC source cannot account for the long-range movement of *Xnr1* and *Lefty*. Therefore, a prospective *Xnr1* movement of, conservatively, 500  $\mu\text{m}$  in 5 hours (Fig. 5) results in no need to invoke additional mechanisms to speed up Nodal autoregulatory spreading. This is particularly important considering that a single *Xnr1* gene is active in tailbud stages, versus the transcriptional relay between multiple *Xnrs* existing during blastula-gastrula (in which we speculate a reduced effect of ECM interaction).

### Ligand processing and clearance

Our assays relied upon expressing epitope-tagged proteins from AC grafts, an approach chosen because of the lack of high signal-to-noise antibodies, and the likely low levels of endogenous *Xnr1* and *Lefty*. Our biochemical analysis strongly supports the idea that the predominant *Xnr1* and *Lefty* molecules moving around the embryo represent properly processed ligands. Such analysis, to our knowledge, has not been performed previously and is important in several respects. First, our method did not overwhelm the secretion or proprotein-processing capacities of source/host tissues and, second, the signal detected and perdurance/clearance estimates reflect, for *Xnr1* and *Lefty*, properties of the mature, glycosylated ligands. We cannot rule out that, ultimately, the dynamics of movement of the natural ligands differ from those determined here, but we did compare functional proteins carrying identical Myc tags. It is possible that a larger tag (e.g. GFP) would more dramatically alter ligand movement and ECM association; moreover, our experiments showed inactivity for *Xnr1*<sup>GFP</sup> and *Lefty*<sup>GFP</sup> (see Fig. S4 in the supplementary material). A complete understanding of mechanisms regulating ligand movement and tissue responses could require developing new tools and methods for precisely detecting ligand that is ECM-bound or 'freely moving', versus engaged at its receptor, for quantitative correlation with downstream events such as nuclear translocation of phospho-Smad2.

### Structural predisposition of splanchnic and somatic LPM to Nodal signaling

The differential distribution of ECM components at somatic-epidermal compared with splanchnic-endodermal interfaces (laminin, HSPG and fibronectin are higher in somatic LPM ECM) may be associated with initiating or maintaining the squamous or columnar cell shapes inherent to each LPM layer. A future goal is to determine how Nodal signaling causes unilateral alterations in LPM cell shape (probably those in the splanchnic layer after formation of the coelom), the degree to which they are broad-ranging or focal, and how they cue and drive asymmetric morphogenesis. Differential cell shape alterations between left and right splanchnic LPM have been linked to chick midgut chirality (Davis et al., 2008). Indeed, the formation of a columnar splanchnic layer may be a structural prerequisite for enacting the cell shape rearrangements preceding asymmetric morphogenesis: *Nkx3.2*-null mice do not form columnar splanchnic cells, with subsequently disrupted asymmetric anatomy (Hecksher-Sørensen et al., 2004).

### Acknowledgements

We thank Pierre McCrea and Douglas DeSimone for antibodies, Michael Ray for technical assistance, Guoqiang Gu and Anna Means for critical feedback, and particularly J. J. Westmoreland and Jessica Sweatt for technical and

conceptual input. Data analyses, in part, used the VUMC Cell Imaging Shared Resource. Supported by NIH R01-GM56238 and Training Program in Developmental Biology T32-HD007502. Deposited in PMC for release after 12 months.

### Competing interests statement

The authors declare no competing financial interests.

### Supplementary material

Supplementary material for this article is available at <http://dev.biologists.org/lookup/suppl/doi:10.1242/dev.056010/-/DC1>

### References

- Aw, S. and Levin, M. (2009). Is left-right asymmetry a form of planar cell polarity? *Development* **136**, 355-366.
- Belenkaya, T. Y., Han, C., Yan, D., Opoka, R. J., Khodoun, M., Liu, H. and Lin, X. (2004). Drosophila Dpp morphogen movement is independent of dynamin-mediated endocytosis but regulated by the glypican members of heparan sulfate proteoglycans. *Cell* **119**, 231-244.
- Bernfield, M., Gotte, M., Park, P. W., Reizes, O., Fitzgerald, M. L., Lincecum, J. and Zako, M. (1999). Functions of cell surface heparan sulfate proteoglycans. *Annu. Rev. Biochem.* **68**, 729-777.
- Bowes, J., Snyder, K., Segerdell, E., Jarabek, C., Azam, K., Zorn, A. and Vize, P. (2010). Xenbase: gene expression and improved integration. *Nucleic Acids Res.* **38**, D607-D612.
- Branford, W. W. and Yost, H. J. (2002). Lefty-dependent inhibition of Nodal- and Wnt-responsive organizer gene expression is essential for normal gastrulation. *Curr. Biol.* **12**, 2136-2141.
- Casey, B. (1998). Two rights make a wrong: human left-right malformations. *Hum. Mol. Genet.* **7**, 1565-1571.
- Casey, B. and Hackett, B. P. (2000). Left-right axis malformations in man and mouse. *Curr. Opin. Genet. Dev.* **10**, 257-261.
- Cha, Y., Takahashi, S. and Wright, C. (2006). Cooperative non-cell and cell autonomous regulation of Nodal gene expression and signaling by Lefty/Antivin and Brachyury in *Xenopus*. *Dev. Biol.* **290**, 246-264.
- Chen, Y. and Schier, A. F. (2001). The zebrafish Nodal signal Squint functions as a morphogen. *Nature* **411**, 607-610.
- Cui, Y., Hackenmiller, R., Berg, L., Jean, F., Nakayama, T., Thomas, G. and Christian, J. L. (2001). The activity and signaling range of mature BMP-4 is regulated by sequential cleavage at two sites within the prodomain of the precursor. *Genes Dev.* **15**, 2797-2802.
- Davis, N., Kurpios, N., Sun, X., Gros, J., Martin, J. and Tabin, C. (2008). The chirality of gut rotation derives from left-right asymmetric changes in the architecture of the dorsal mesentery. *Dev. Cell* **15**, 134-145.
- Deimling, S. J. and Drysdale, T. A. (2009). Retinoic acid regulates anterior-posterior patterning within the lateral plate mesoderm of *Xenopus*. *Mech. Dev.* **126**, 913-923.
- Dzamba, B. J., Jakab, K. R., Marsden, M., Schwartz, M. A. and DeSimone, D. W. (2009). Cadherin adhesion, tissue tension, and noncanonical Wnt signaling regulate fibronectin matrix organization. *Dev. Cell* **16**, 421-432.
- García-García, M. J. and Anderson, K. V. (2003). Essential role of glycosaminoglycans in Fgf signaling during mouse gastrulation. *Cell* **114**, 727-737.
- Guo, Z. and Wang, Z. (2009). The glypican Dally is required in the niche for the maintenance of germline stem cells and short-range BMP signaling in the *Drosophila* ovary. *Development* **136**, 3627-3635.
- Hamada, H. (2008). Breakthroughs and future challenges in left-right patterning. *Dev. Growth Diff.* **50**, S71-S78.
- Hecksher-Sørensen, J., Watson, R. P., Lettice, L. A., Serup, P., Eley, L., De Angelis, C., Ahlgren, U. and Hill, R. E. (2004). The splanchnic mesodermal plate directs spleen and pancreatic laterality, and is regulated by Bapx1/Nkx3.2. *Development* **131**, 4665-4675.
- Hemmati-Brivanlou, A. and Thomsen, G. H. (1995). Ventral mesodermal patterning in *Xenopus* embryos: expression patterns and activities of BMP-2 and BMP-4. *Dev. Genet.* **17**, 78-89.
- Horne-Badovinac, S., Rebagliati, M. and Stainier, D. Y. R. (2003). A cellular framework for gut-looping morphogenesis in zebrafish. *Science* **302**, 662-665.
- Itoh, K. and Sokol, S. Y. (1994). Heparan sulfate proteoglycans are required for mesoderm formation in *Xenopus* embryos. *Development* **120**, 2703-2711.
- Jing, X., Zhou, S., Wang, W. and Chen, Y. (2006). Mechanisms underlying long- and short-range nodal signaling in Zebrafish. *Mech. Dev.* **123**, 388-394.
- Jones, C. M., Armes, N. and Smith, J. C. (1996). Signalling by TGF-beta family members: short-range effects of *Xnr-2* and BMP-4 contrast with the long-range effects of activin. *Curr. Biol.* **6**, 1468-1475.
- Kramer, K. L. and Yost, H. J. (2002). Ectodermal syndecan-2 mediates left-right axis formation in migrating mesoderm as a cell-nonautonomous Vg1 cofactor. *Dev. Cell* **2**, 115-124.

- Kramer, K. L., Barnette, J. E. and Yost, H. J. (2002). PKCgamma regulates syndecan-2 inside-out signaling during *Xenopus* left-right development. *Cell* **111**, 981-990.
- Kucenas, S., Takada, N., Park, H.-C., Woodruff, E., Broadie, K. and Appel, B. (2008). CNS-derived glia ensheath peripheral nerves and mediate motor root development. *Nat. Neurosci.* **11**, 143-151.
- Le Good, J. A., Joubin, K., Giraldez, A. J., Ben-Haim, N., Beck, S., Chen, Y., Schier, A. F. and Constam, D. B. (2005). Nodal stability determines signaling range. *Curr. Biol.* **15**, 31-36.
- Lowe, L. A., Supp, D. M., Sampath, K., Yokoyama, T., Wright, C. V., Potter, S., Overbeek, P. and Kuehn, M. R. (1996). Conserved left-right asymmetry of nodal expression and alterations in murine situs inversus. *Nature* **381**, 158-161.
- Lugemwa, F. N. and Esko, J. D. (1991). Estradiol beta-D-xyloside, an efficient primer for heparan sulfate biosynthesis. *J. Biol. Chem.* **266**, 6674-6677.
- Massagué, J. (1998). TGF-beta signal transduction. *Annu. Rev. Biochem.* **67**, 753-791.
- McDowell, N., Zorn, A. M., Crease, D. J. and Gurdon, J. B. (1997). Activin has direct long-range signalling activity and can form a concentration gradient by diffusion. *Curr. Biol.* **7**, 671-681.
- Meier, S. (1979). Development of the chick embryo mesoblast. Formation of the embryonic axis and establishment of the metamer pattern. *Dev. Biol.* **73**, 24-45.
- Nakamura, T., Mine, N., Nakaguchi, E., Mochizuki, A., Yamamoto, M., Yashiro, K., Meno, C. and Hamada, H. (2006). Generation of robust left-right asymmetry in the mouse embryo requires a self-enhancement and lateral-inhibition system. *Dev. Cell* **11**, 495-504.
- Nieuwkoop, P. D. and Faber, J. (1967). *Normal Table of Xenopus laevis: A Systematical and Chronological Survey of the Development from the Fertilized Egg till the End of Metamorphosis*. Amsterdam: North-Holland Publishing Company.
- Ohi, Y. and Wright, C. (2007). Anteriorward shifting of asymmetric Xnr1 expression and contralateral communication in left-right specification in *Xenopus*. *Dev. Biol.* **301**, 447-463.
- Ohkawara, B., Iemura, S.-i., ten Dijke, P. and Ueno, N. (2002). Action range of BMP is defined by its N-terminal basic amino acid core. *Curr. Biol.* **12**, 205-209.
- Oki, S., Hashimoto, R., Okui, Y., Shen, M. M., Mekada, E., Otani, H., Saijoh, Y. and Hamada, H. (2007). Sulfated glycosaminoglycans are necessary for Nodal signal transmission from the node to the left lateral plate in the mouse embryo. *Development* **134**, 3893-3904.
- Pohl, B. S., Rössner, A. and Knöchel, W. (2005). The Fox gene family in *Xenopus laevis*: FoxI2, FoxM1 and FoxP1 in early development. *Int. J. Dev. Biol.* **49**, 53-58.
- Ramsdell, A. (2005). Left-right asymmetry and congenital cardiac defects: Getting to the heart of the matter in vertebrate left-right axis determination. *Dev. Biol.* **288**, 1-20.
- Raya, Á. and Belmonte, J. C. I. (2006). Left-right asymmetry in the vertebrate embryo: from early information to higher-level integration. *Nat. Rev. Genet.* **7**, 283-293.
- Sakuma, R., Ohnishi, Y., Y.-i., Meno, C., Fujii, H., Juan, H., Takeuchi, J., Ogura, T., Li, E., Miyazono, K. and Hamada, H. (2002). Inhibition of Nodal signalling by Lefty mediated through interaction with common receptors and efficient diffusion. *Genes Cells* **7**, 401-412.
- Sampath, K., Cheng, A. M., Frisch, A. and Wright, C. V. (1997). Functional differences among *Xenopus* nodal-related genes in left-right axis determination. *Development* **124**, 3293-3302.
- Schier, A. F. (2003). Nodal signaling in vertebrate development. *Annu. Rev. Cell Dev. Biol.* **19**, 589-621.
- Scholpp, S. and Brand, M. (2004). Endocytosis controls spreading and effective signaling range of Fgf8 protein. *Curr. Biol.* **14**, 1834-1841.
- Schweickert, A., Weber, T., Beyer, T., Vick, P., Bogusch, S., Feistel, K. and Blum, M. (2007). Cilia-driven leftward flow determines laterality in *Xenopus*. *Curr. Biol.* **17**, 60-66.
- Sive, H. L., Grainger, R. M. and Harland, R. M. (2000). *Early Development of Xenopus laevis: A Laboratory Manual*. Cold Spring Harbor, NY: Cold Spring Harbor Laboratory Press.
- Slack, J. M. and Tannahill, D. (1992). Mechanism of anteroposterior axis specification in vertebrates. Lessons from the amphibians. *Development* **114**, 285-302.
- Stevens, R. L. and Austen, K. F. (1982). Effect of p-nitrophenyl-beta-D-xyloside on proteoglycan and glycosaminoglycan biosynthesis in rat serosal mast cell cultures. *J. Biol. Chem.* **257**, 253-259.
- Tabin, C. (2006). The key to left-right asymmetry. *Cell* **127**, 27-32.
- Turing, A. M. (1990). The chemical basis of morphogenesis. 1953. *Bull. Math. Biol.* **52**, 119-153.
- Wallingford, J. B., Rowning, B. A., Vogeli, K. M., Rothbacher, U., Fraser, S. E. and Harland, R. M. (2000). Dishevelled controls cell polarity during *Xenopus* gastrulation. *Nature* **405**, 81-85.
- Wang, X. and Yost, H. J. (2008). Initiation and propagation of posterior to anterior (PA) waves in zebrafish left-right development. *Dev. Dyn.* **237**, 3640-3647.
- Westmoreland, J. J., Takahashi, S. and Wright, C. V. E. (2007). *Xenopus* Lefty requires proprotein cleavage but not N-linked glycosylation to inhibit Nodal signaling. *Dev. Dyn.* **236**, 2050-2061.
- Williams, P. H., Hagemann, A., González-Gaitán, M. and Smith, J. C. (2004). Visualizing long-range movement of the morphogen Xnr2 in the *Xenopus* embryo. *Curr. Biol.* **14**, 1916-1923.
- Wright, C. V. (2001). Mechanisms of left-right asymmetry: what's right and what's left? *Dev. Cell* **1**, 179-186.
- Yamamoto, M., Mine, N., Mochida, K., Sakai, Y., Saijoh, Y., Meno, C. and Hamada, H. (2003). Nodal signaling induces the midline barrier by activating Nodal expression in the lateral plate. *Development* **130**, 1795-1804.
- Yost, H. J. (1990). Inhibition of proteoglycan synthesis eliminates left-right asymmetry in *Xenopus laevis* cardiac looping. *Development* **110**, 865-874.
- Yu, S. R., Burkhardt, M., Nowak, M., Ries, J., Petrasek, Z., Scholpp, S., Schwill, P. and Brand, M. (2009). Fgf8 morphogen gradient forms by a source-sink mechanism with freely diffusing molecules. *Nature* **461**, 533-536.